UNIVERSITAT DE BARCELONA

FUNDAMENTAL PRINCIPLES OF DATA SCIENCE MASTER'S THESIS

Developing an Early-warning system for Acute Myocardial Infractions in Catalonia

Author:
Gabriela ZEMENČÍKOVÁ

Supervisor:
Xavier Rodó,
Alejandro Fontal,
Laura Igual Muñoz

A thesis submitted in partial fulfillment of the requirements for the degree of MSc in Fundamental Principles of Data Science

in the

Facultat de Matemàtiques i Informàtica

June 23, 2024

UNIVERSITAT DE BARCELONA

Abstract

Facultat de Matemàtiques i Informàtica

MSc

Developing an Early-warning system for Acute Myocardial Infractions in Catalonia

by Gabriela ZEMENČÍKOVÁ

We aim to investigate the association between temperature, humidity, pollution and the incidence of acute myocardial infarction (AMI) in Catalonia, Spain and set up a new predictor scheme. It is established that both hot and cold temperatures influence the incidence of AMI, the relationship between other environmental variables and AMI, particularly across different seasons, remains not so well understood. However, a predictive modelling scheme is yet lacking. A dataset with 22,812 hospital admissions at the scale of the 948 municipalities in Catalonia stratified by province, sex and age is available for analysis during the interval 2010-2018, together with daily average temperature, pollution and humidity values. We employ two modeling approaches: Seasonal Autoregressive Integrated Moving Average (SARIMA) models and Long Short-Term Memory (LSTM) neural networks. The analysis identifies key environmental predictors of AMI incidence. Our findings underscore the importance of considering environmental factors in public health strategies aimed at reducing AMI risk offering a foundation for future studies and policy-making.

Acknowledgements

Finishing this project would have been impossible without my supervisors, who have provided amazing guidance, support, and interesting insights throughout the project; Nacho, who provided the best coffee and climbing sessions; Ro, who dragged me into the beach occasionally so I wouldn't get too crazy; Karolina and Katarina, who have been very kind to listen to my rants; my family, who still has no clue what I am actually studying; and everyone else, who puts up with me barely being a person these days. A song I want to remember when I find a printed version of this report in 30 years time: *You took your time* by Mount Kimbie and King Krule.

Contents

List of Figures

List of Tables

List of Abbreviations

ADF	Augmented Dickey-Fuller
AMI	Acute Myocardial Infarction
ASIR	Age-Standardized Incidence Rates
CVD	Cardiovascular Disease
ERF	Exposure-Response Function
EWS	Early Warning System
LIME	Local Interpretable Model-agnostic Explanations
LSTM	Long Short-Term Memory
MAE	Mean Absolute Error
MAPE	Mean Absolute Percentage Error
NO2	Nitrogen Dioxide
PM	Particulate Matter
RNN	Recurrent Neural Networks
RMSE	Root Mean Square Error
SARIMA	Seasonal Autoregressive Integrated Moving Average
SARIMAX	Seasonal Autoregressive Integrated Moving Average with Exogenous Variables
SHAP	Shapley Additive Explanations
SMBO	Sequential Model-Based Optimization

Chapter 1

Introduction

Cardiovascular diseases (CVDs) remain a significant public health concern globally, contributing substantially to morbidity and mortality rates. Among the various manifestations of CVDs, acute myocardial infarction (AMI) is not only one of the leading causes of mortality but also it stands out as a critical condition requiring prompt medical attention and intervention. It is defined as myocardial necrosis, which occurs due to decreased coronary blood flow, leading to insufficient oxygen supply to the heart and cardiac ischemia (Mechanic, Gavin, and Grossman, 2024). The interaction between environmental factors having an effect on the incidence of AMI gained an increased attention in recent years, urging researchers to delve deeper into understanding the complexity involved.

In regions characterised by diverse climatic conditions, such as Catalonia, Spain, where temperature fluctuations, humidity levels, and pollution levels exhibit considerable variability across different seasons and different geographical locations, exploring the nexus between environmental parameters and the occurrence of AMI becomes especially relevant. Catalonia, with its unique blend of coastal and inland areas, urban centres, rural landscapes, mountains and sea provides a compelling place for investigating these associations.

The objective of this study is to explain the association between temperature, humidity, pollution, and the incidence of AMI in Catalonia, Spain. The analysis is performed using a dataset encompassing hospital admissions over a time-frame between years 2010 to 2018 across 948 municipalities stratified by province, sex, and age, and daily meteorological and pollution data, that is used to understand the dynamics and interaction of the variables.

While existing literature indicates that both hot and cold temperatures have an impact on the incidence of AMI, the relationship between other environmental variables and AMI, particularly across different seasons, remains less clear. Furthermore, despite advancements in statistical modelling techniques, a comprehensive predictive modelling scheme well-fitted for Catalonia's context is yet to be established.

To address these gaps, this study proposes a multifaceted approach that incorporates two different methodologies, specifically Seasonal Autoregressive Integrated Moving Average Models (SARIMA), and Long Short-Term Memory (LSTM) machine learning algorithms. Combining these models with detailed exploratory analysis of the given dataset, we aim to develop a robust predictive model that captures the relationships between environmental factors and the incidence of AMI in Catalonia.

Considering the climate change, there has been a discussion about the relationship between environmental factors and the incidence of AMI. As the changing of climatic conditions impact cardiovascular health, through this interdisciplinary approach, we aim to enhance our understanding of the environmental determinants

of AMI. Moreover, this thesis should provide policymakers and healthcare practitioners with valuable insights to mitigate the issue of cardiovascular diseases in Catalonia and to address the dynamic challenges posed by climate change on public health.

Furthermore, Catalonia's diverse geographical and demographic landscape provides an opportunity to investigate potential spatial and demographic variations in the relationship between environmental factors and AMI incidence. By stratifying our analysis by province, sex, and age groups, there is a potential to explore any disparities or differential susceptibility to environmental variables and potential triggers across different segments of the population. As a result, understanding the dynamics can help to create interventions that would be aimed at specific most susceptible group and reduce the incidence and impact of AMI in Catalonia.

This paper is structured to provide a comprehensive analysis of the relationship between environmental factors and AMI incidence. A section 2 begins with a detailed data analysis, describing the sources of our hospital admissions, meteorological, and pollution datasets, followed by the data wrangling process and exploratory data analysis to uncover initial patterns and relationships. A section 3 is a methodology section that outlines the theoretical framework of the SARIMA and LSTM models used in this study, along with the process of hyperparameter optimization to enhance model performance. In the results section, section 4, we present the evaluation of the models, including a comparison of suitable models based on various performance metrics, and discuss the predictive capabilities of each model while identifying key environmental variables influencing AMI incidence. We then acknowledge the limitations of our study, such as potential data quality issues and the assumptions inherent in our modeling approaches. Finally in section 5, the paper concludes with a summary of our findings, their implications for public health strategies, and suggestions for future research to further investigate the dynamics between environmental factors and cardiovascular health outcomes.

Chapter 2

Data Analysis

2.1 Data Sources

For the purposes of the analysis there have been various data sources used. The environmental dataset Catalonia under investigation composed of temperature, relative humidity, air pollution data, and census data Catalonia was obtained from the Statistical Institute Catalonia. The census data was obtained from the population estimates, which provides updates every six months at the county level for 5-year age groups stratified by sex.

Air pollution metrics were collected from a network of 90 monitoring stations dispersed across Catalonia, as shown in Figure 2.2a. These stations provide comprehensive coverage of atmospheric conditions across the regions. Hourly readings of each pollutant were aggregated to daily observations for analysis. There were various contaminants measured, specifically benzene, chlorine, carbon monoxide, hydrogen sulfide, mercury, nitric oxide, nitrogen dioxide, nitrogen oxides, ozone, particular matter and sulfur dioxide. However, only ozone and PM10 were selected for the study due to the inconsistent measurement of all contaminants across stations and a significant amount of missing data for some pollutants (for more details see Figure 2.1).

Similarly, meteorological observations, including outdoor temperature and relative humidity, were collected from 239 meteorological stations distributed throughout Catalonia, as illustrated in Figure 2.2b. Raw measurements, initially recorded at half-hour intervals, were aggregated to daily data points to perform the analysis. There were no missing data.

The AMI dataset was obtained from ten main hospitals across Catalonia. Even though, the dataset contains detailed spatial information, including the postal code of residence for each patient, it is necessary to aggregate the data to a higher level of spatial resolution to recognise meaningful patterns. Furthermore, the data is stratified by age and sex of each hospitalised patient. Our initial approach involved aggregating the data to the county-level (comarques) and higher-level territories (àmbits territorials) within Catalonia. However, we encountered limitations when working with county-level data, as some counties yielded sparse observations, often with only one or no cases of AMI recorded per day for many counties. This limited data density hindered our ability to extract meaningful insights and detect significant trends. As a reason, we used higher-level regional territories.

2.2 Data Exploration

The complex dynamics of factors influencing the incidence of AMI necessitates a multifaceted approach. This exploratory analysis delves into several key factors that

FIGURE 2.1: Missing data in pollutants Over time

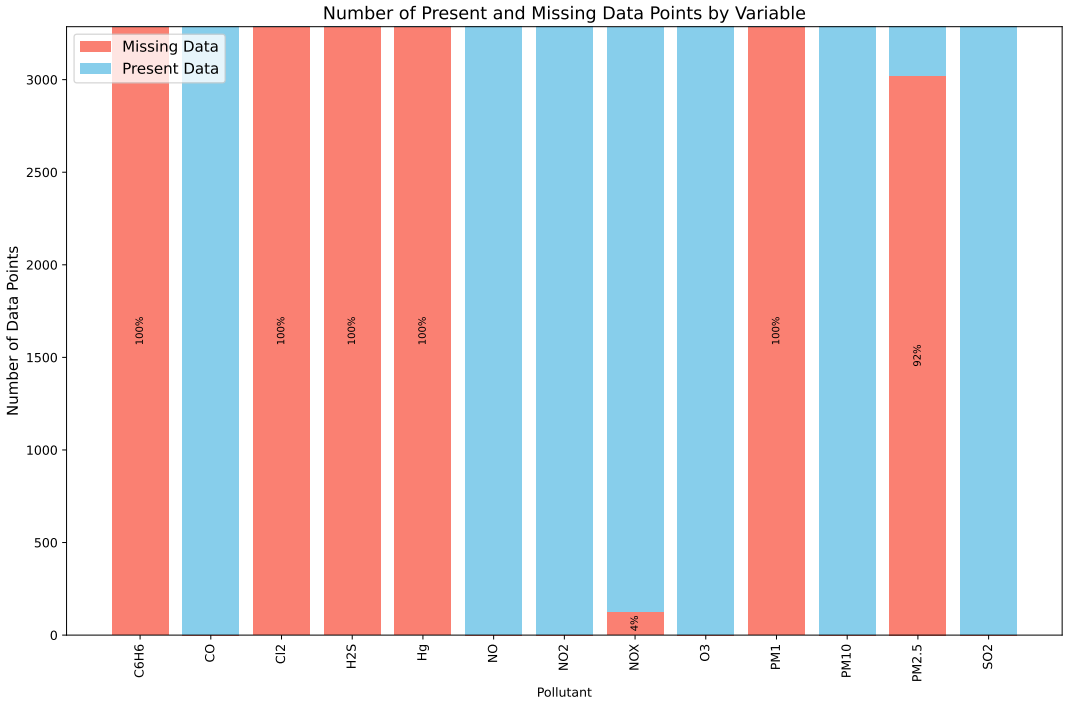

may contribute to variations in AMI incidence within Catalonia, Spain. In this section, the exploratory analysis is shown on aggregated data for the separate high-level regions.

As noted by Mechanic, Gavin, and Grossman (2024) there are many risk factors potentially contributing to the occurrence of AMI. Considering the set of non-modifiable risk factors that include factors such as sex and age. The further analysis of associations of these variables was conducted by Canto et al. (2012).

2.2.1 Sex and Age as Significant Factors

The role of sex as an important factor in the epidemiology of AMI is well established. Sexual dimorphism in cardiovascular physiology and pathophysiology underpins the differential risk profiles observed in males and females (Zhang et al., 2012). While men traditionally exhibit a higher overall incidence of AMI, women often present with AMI at older ages and experience worse outcomes, including higher mortality rates. Furthermore, women are more susceptible to the effects of air pollution given sex differences in air pollution lung deposition, and because a greater proportion of women have airway hyper-responsiveness than men. Hormonal influences, anatomical differences, and variations in risk factor prevalence contribute to these sex-specific disparities (Čulić et al., 2002). In order to explore the role of sex in AMI incidence within Catalonia, it is necessary to disaggregate data by sex and examine potential differences in risk factor profiles, symptom presentation, and healthcare utilisation patterns between males and females.

Age is a significant predictor of AMI incidence. Exploratory analysis together with previous academic findings suggest that there are certain age groups which are more susceptible to the effects environmental factors. The risk increases with

FIGURE 2.2: Spatial Distribution of Monitoring Stations

(A) Spatial Distribution of Air Pollution

(B) Spatial Distribution of Meteorological variables

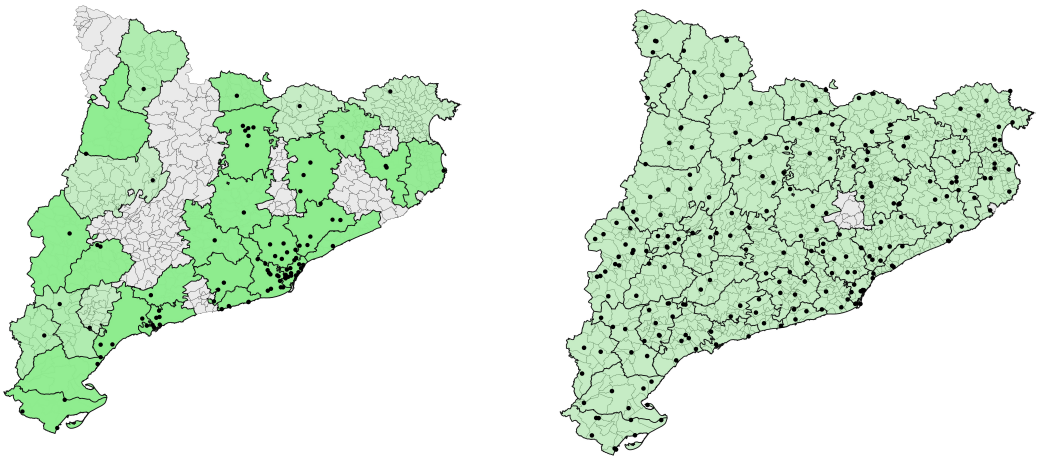

advancing age. Age-related changes in cardiovascular structure and function, coupled with the cumulative effects of traditional risk factors such as hypertension, diabetes, and dyslipidemia, contribute to the elevated AMI risk observed in older adults (Mehta et al., 2001). In order to explore age-specific trends in AMI incidence within Catalonia, it is necessary to stratify the population into distinct age groups and analyse age-specific incidence rates, temporal trends, and clinical characteristics. This will enable the identification of age-specific risk factors and vulnerabilities.

Figure 2.3 displays the AMI alerts distribution by sex and age. We can observe that the distribution differs when comparing both genders. The highest number of AMI alerts when it comes to females is around their eighties. On the other side, when it comes to men their peak is around fifties. Both of these results are consistent with the previous paragraph. It suggests that there is some dependence on population structure. Thus, when dis-aggregating data spatially for any given area, there is a need to take into account the population structure.

Since we are dealing with dataset during various years, there is a need to examine the overall trend of the series. As we assume that both sex and age may be a potential factors of AMI alerts, we should take into consideration the changes in population structures in the examined period. In other words, dealing with population structure, there is a potential of ageing population that could be present in the data. Figure 2.4 shows the development of AMI alerts in 2010 and 2018 and the population structure. It can be observed that the overall increasing long-term trend of AMI alerts and ageing of the population are somehow correlated. By combining both variables, we calculate AMI incidence rate as plotted in Figure 2.5. By examining the age-sex specific incidence rates we can observe that the incidence of AMI in Catalonia has exhibited an increasing trend over the years, indicating a complex dynamics of various factors beyond changes in population structure alone. This means that, even after controlling for age, we should observe an increase in the incidence of age-group specific AMI events over the years.

Upon examining the yearly incidences for age and sex groups, we proceeded to fit a linear regression model for the yearly incidence of each group and plotted the slope of the regression line along with the 95% confidence interval. While the slope

FIGURE 2.3: Age and sex distribution of all AMI alerts (2010-2018)

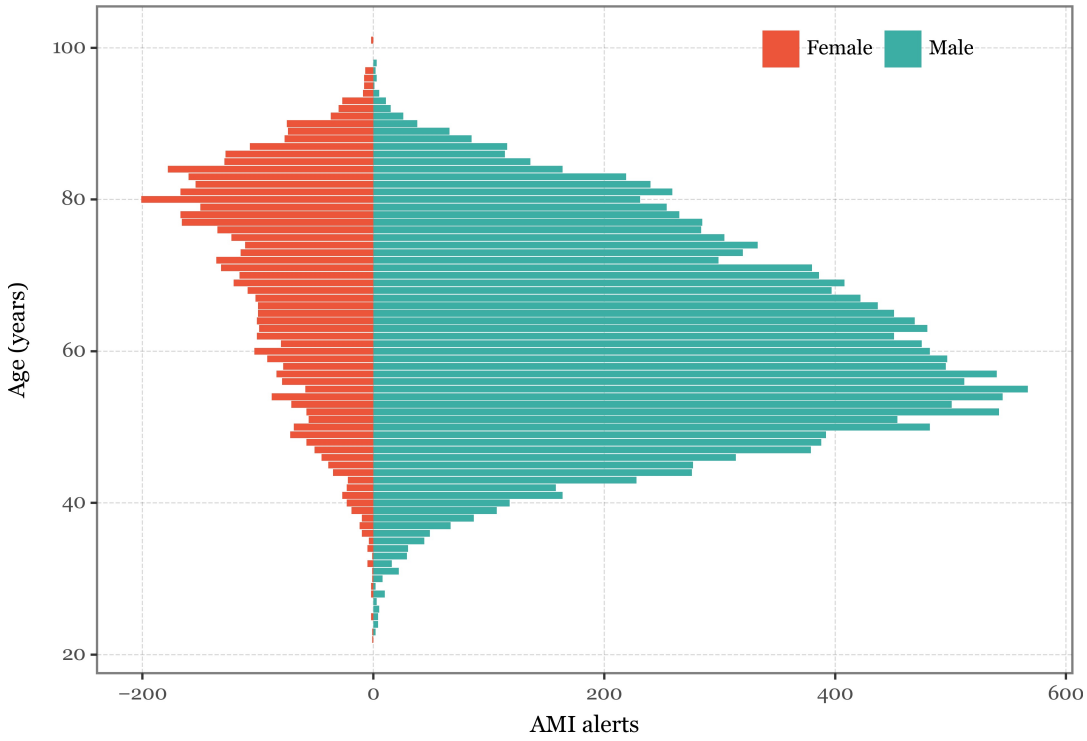

for many age and sex groups is not significantly different from zero, certain groups show a significant increase. Specifically, we found that males aged 50 to 64 and 75 to 94, and females aged 55 to 64 and 85 to 89, exhibited a significant trend at a 95% confidence level (see Table C.1 in Appendix B). Combining all information together, we proceed and define our target variable.

2.2.2 Choice of Age-Standardized Incidence Rates (ASIR)

In the analysis of AMI incidence, researchers often face the challenge of comparing incidence rates across populations with different age distributions. As mentioned in the previous subsections, the raw incidence rate of AMI may be influenced by demographic factors, i.e. differences in the age structure of the populations under study, making direct comparisons problematic. To address this issue, we choose to use Age-Standardized Incidence Rates (ASIR), which adjust for differences in age distribution across populations.

ASIR is a useful metric for comparing disease incidence rates between populations or over time while accounting for differences in age structure. By standardizing incidence rates to a reference population with a standard age distribution, ASIR enables fair comparisons across populations with different age profiles. This adjustment helps to isolate the underlying differences in disease burden attributable to factors other than age distribution, facilitating more meaningful comparisons and interpretations.

In the context of our analysis on the association between environmental factors and AMI incidence in Catalonia, Spain, the use of ASIR offers several advantages. Catalonia encompasses diverse demographic profiles across its municipalities, with variations in age distribution that may influence the observed AMI incidence rates.

FIGURE 2.4: Development of Population (2010 - 2018)

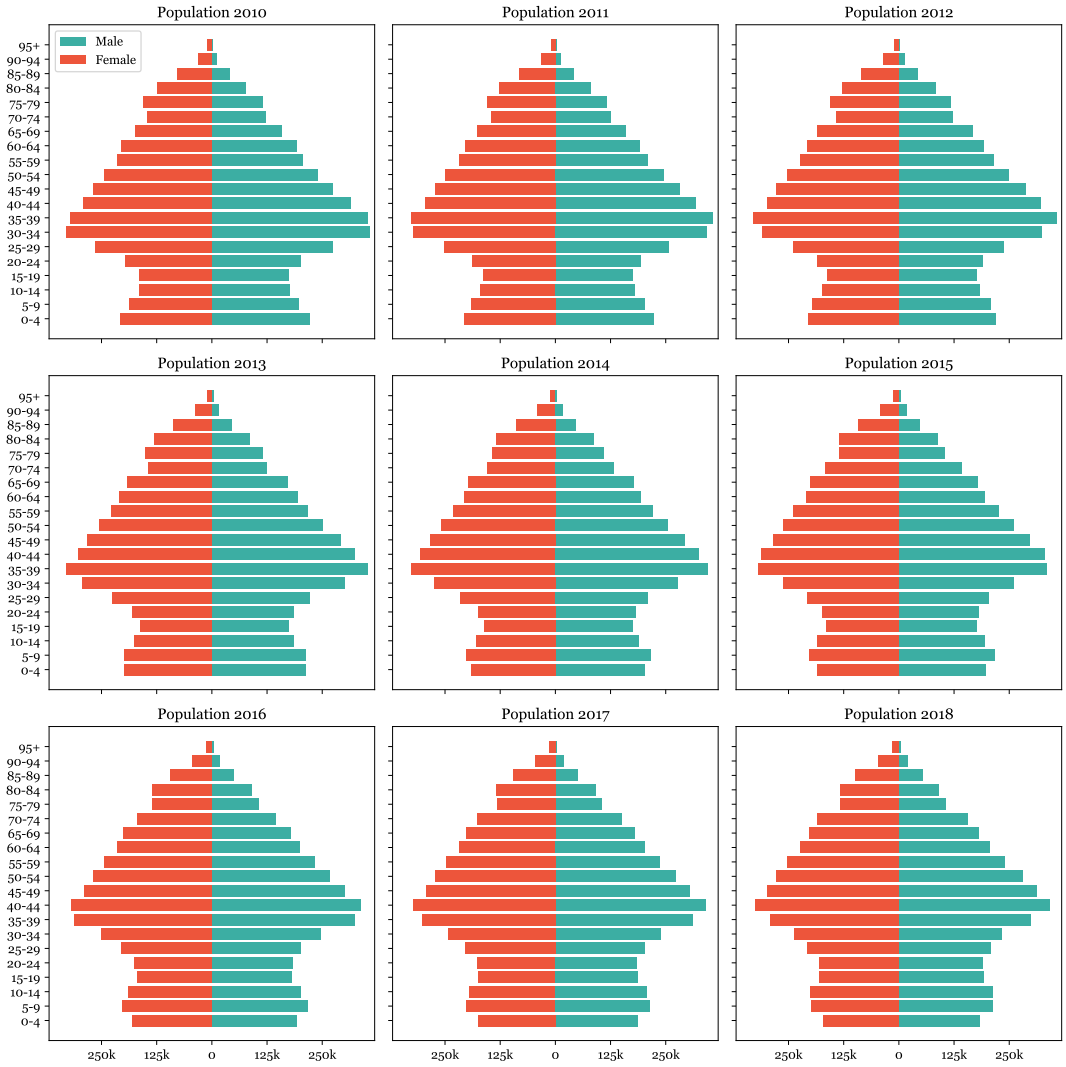

By standardizing AMI incidence rates to a reference population, such as the World Health Organization (WHO) standard population, we can obtain ASIR estimates that account for differences in age distribution, enabling more robust comparisons of AMI incidence across municipalities and over time.

Our analysis begins with the estimation of AMI incidence over a year, stratified by 5-year age groups and sex, utilizing comprehensive datasets. Subsequently, population distributions sourced from IDESCAT are employed to compute the expected number of AMI events for each region and year. By juxtaposing these expected values with the actual observed events, we can discern trends in AMI incidence that are independent of demographic influences, providing a nuanced understanding of underlying patterns.

The calculation of ASIR represents a pivotal step in standardizing incidence rates to a reference population, thereby facilitating equitable comparisons across regions and temporal intervals. This standardization process effectively mitigates the confounding effects of age and sex distributions, enabling a more accurate assessment of true changes in AMI incidence. ASIR serves as a robust analytical tool, offering

FIGURE 2.5: Development of Incidence Rate per 100k (2010 - 2018)

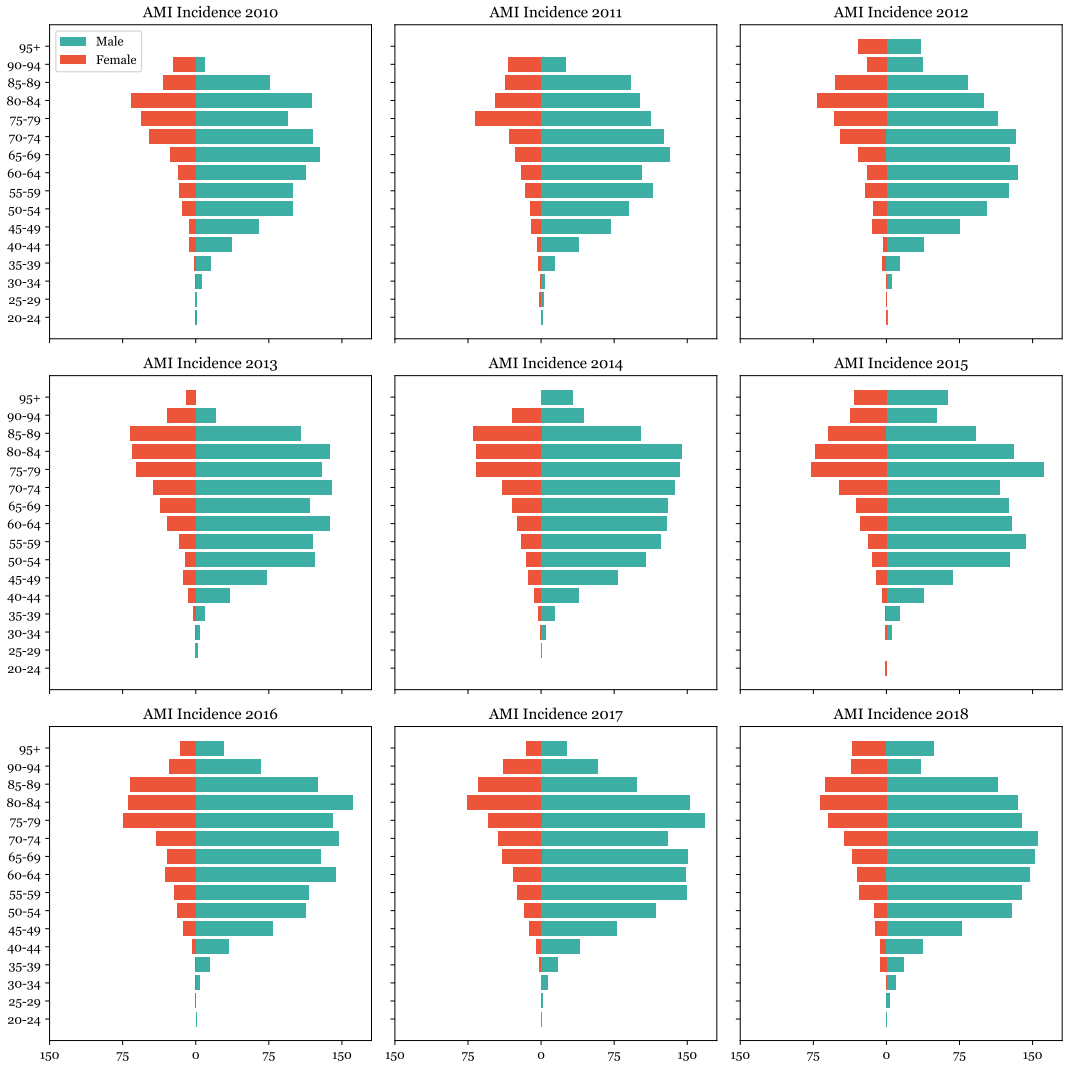

insights into the temporal evolution of AMI incidence while controlling for demographic heterogeneity.

Visualization of raw AMI case data reveals intricate temporal patterns, including daily, weekly, monthly, and yearly fluctuations. These patterns, while indicative of potential seasonal variations and long-term trends, may also be influenced by shifts in population demographics. By employing ASIR, we aim to mitigate the changes in AMI incidence from demographic effects.

In summary, the choice of ASIR over raw AMI incidence rates in our analysis helps to mitigate the confounding effect of age distribution on the observed incidence rates. By standardizing incidence rates to a reference population, ASIR facilitates more accurate comparisons of disease burden across populations with different age structures, enhancing the validity and interpretability of our findings. Before examining ASIR closely, it is crucial to analyse data spatially.

2.2.3 Spatial Distribution of AMI Incidence

In this subsection, we explore the spatial distribution of AMI incidence across counties and territorial regions in Catalonia. By examining the geographical variability of AMI incidence rates and adjusting for population differences, we aim to identify patterns and trends that may inform targeted public health interventions and resource allocation strategies. The geographical distribution of AMI incidence within Catalonia is influenced by a myriad of factors, including urbanisation, socioeconomic status, healthcare infrastructure, and environmental exposures. Urban centres may exhibit higher AMI incidence rates due to the concentration of risk factors such as sedentary lifestyles, unhealthy dietary habits, and air pollution. Conversely, rural areas may face challenges related to limited access to healthcare services and longer transport times to medical facilities.

Counties

First, we examine the AMI alerts per 100,000 inhabitants for each county and year. This analysis reveals substantial variability across counties, indicating heterogeneous AMI incidence rates within Catalonia. Moreover, the observed trends in AMI incidence appear consistent across all counties, suggesting the presence of region-wide patterns.

However, reporting AMI incidence per 100,000 inhabitants may skew results if not accounting for population structure differences among counties. To address this limitation, we compute the expected number of cases for each county and year using the respective population structures. Subsequently, we calculate the ASIR for each county and year, providing a more accurate representation of AMI incidence that adjusts for demographic variations.

Visualizing the ASIR for each county and year offers insights into the spatial distribution of AMI incidence rates, facilitating comparisons across regions and revealing areas of elevated risk. By accounting for population differences, ASIR enables a more precise assessment of AMI incidence trends, aiding in the identification of high-risk areas and the implementation of targeted interventions.

Àmbits Territorials

Next, we extend our analysis to the territorial regions (àmbits territorials) in Catalonia, which offer larger and more stable geographical units for examination. Similar to the county-level analysis, we compute AMI incidence rates per 100,000 inhabitants for each territorial region and year.

The analysis reveals an increase in AMI incidence rates across all territorial regions, accompanied by significant spatial variability within each year. However, differences in population structure among territorial regions may influence observed incidence rates. To address this issue, we compute the expected number of cases for each territorial region and year using population data.

Subsequently, we calculate the ASIR for each territorial region and year, enabling a comprehensive assessment of AMI incidence trends while adjusting for demographic differences. The analysis highlights areas with elevated ASIR, indicating regions of heightened AMI risk.

By comparing expected and observed AMI incidence rates, we identify deviations from expected trends, providing valuable insights into spatial patterns of AMI

occurrence. This information can inform targeted public health interventions and resource allocation efforts, ultimately contributing to the prevention and management of AMI at a regional level.

When exploring detailed temporal patterns in Age-Standardized Incidence Rates (ASIR) across territorial regions (ATs), we encounter challenges due to the varying population sizes and the resulting noise in the data. With the metropolitan area of Barcelona housing a significant portion of Catalonia's population, the distribution of AMI alerts across ATs differs greatly, leading to discrepancies in signal strength. Given that the yearly incidence of AMI alerts ranges from 30 to 40 cases per year per 100,000 inhabitants, the signal-to-noise ratio in the least populated areas becomes notably skewed, rendering analysis at the daily scale impractical. For reference, the Table **??** illustrates the total number of AMI alerts for each AT and year.

TABLE 2.1: AMI alerts by AT and year

AT		Year								
		2010	2011	2012	2013	2014	2015	2016	2017	2018
AT01	Metropolità	1401	1469	1574	1582	1629	1663	1697	1826	1820
AT02	Comarques Gironines	192	165	218	265	245	258	268	277	306
AT03	Camp de Tarragona	103	87	134	164	161	190	181	214	216
AT04	Terres de l'Ebre	34	42	37	61	52	66	65	77	66
AT05	Ponent	82	103	107	99	95	112	107	120	135
AT06	Comarques Centrals	152	138	144	154	171	172	172	175	201
AT07	Alt Pirineu i Aran	16	21	29	23	25	19	30	23	34
AT08	Penedès	98	108	133	127	162	157	181	190	189

To address this issue of high variability, we utilize moving averages to smooth the ASIR data and extract hidden trends while minimizing the impact of short-term fluctuations. By interpolating the expected daily AMI alerts based on population estimates for every 6 months in each AT and computing daily ASIR moving averages, we obtain a cleaner signal that enables a more precise assessment of temporal patterns in AMI incidence across territorial regions.

Moving average indicates that the current value is linearly dependent on the following terms - the series mean, the current and previous error terms (Peixeiro, 2022). This approach allows us to discern underlying trends and variations in AMI occurrence, facilitating a more comprehensive understanding of spatial and temporal patterns in AMI epidemiology. Mathematically, it is expressed as

$$y_t = \mu + \varepsilon_t + \theta_1 \varepsilon_{t-1} + \theta_2 \varepsilon_{t-2} + \cdots + \theta_q \varepsilon_{t-q}$$

where:

- y_t represents the value of the time series at time t,
- μ is the mean of the time series,
- ε_t denotes the error term or random shock at time t,
- $\theta_1, \theta_2, \ldots, \theta_q$ are the parameters of the model representing the coefficients of past error terms,
- q is the order of the moving average model, indicating how many past error terms are included in the model.

For smoothing ASIR by using moving averages of different number of days see Figure 2.6. From the figure, we can slightly observe a long-term trend with several peaks within the examined period and also the is an apparent cyclical pattern in the data.

There is a clear seasonal patter in the series. The ASIR is higher during the beginning and end of the year and lower in the summer months. Also, we decomposed the series to make sure the seasonal component was present (Figure C.1 in Appendix C. We can see the long-term change in the series which presents increase over time, the seasonal pattern which we can see an annual repeated fluctuations. It is important to note that when smoothing the data there is a need for a balance between the noise reduction and still maintaining the integrity of the original data. Thus, the data will be aggregated on a weekly level.

FIGURE 2.6: Moving Averages of ASIR Over Time

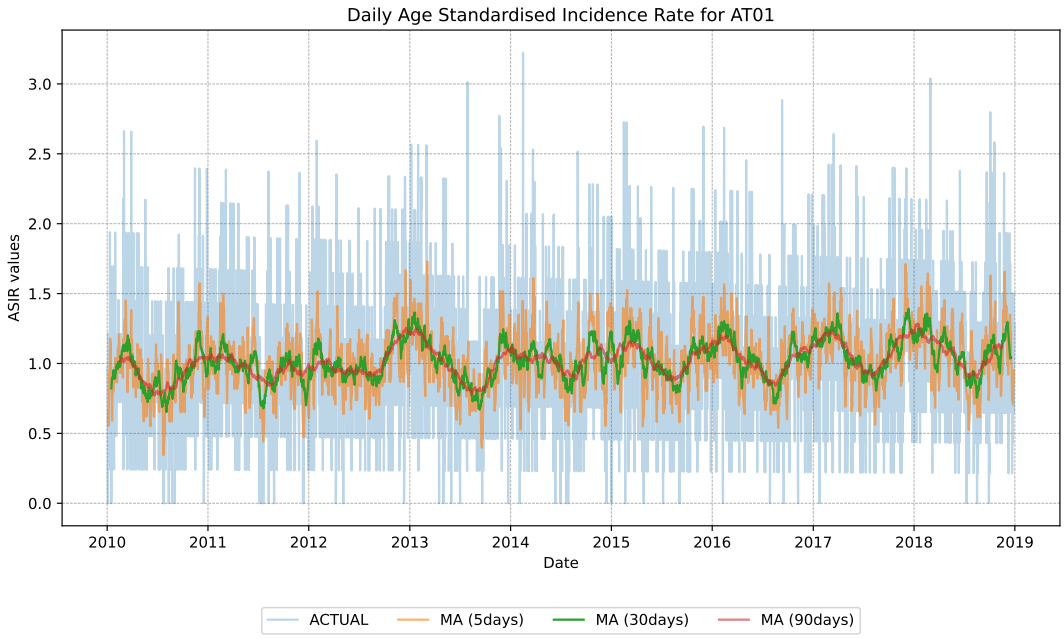

2.2.4 Seasonal Variations and Weather Patterns

There is a growing body of evidence indicating that seasonal variations in weather conditions, such as temperature, humidity, and air pollution levels, are associated with fluctuations in AMI incidence. These fluctuations are particularly evident between winter and summer months. Cold temperatures and winter-related factors, including respiratory infections, holiday stress, and changes in physical activity and dietary habits, may contribute to a higher incidence of AMI during winter months. Conversely, high temperatures and summer-related factors, such as dehydration, outdoor physical exertion, and increased air pollution levels, may exacerbate cardiovascular risk during summer months.

To analyze seasonal trends in AMI incidence within Catalonia, it is necessary to assess the temporal patterns of AMI occurrence, identify seasonal peaks and troughs, and explore potential interactions between weather variables and cardiovascular risk factors. In order to proceed, the data has been split into two seasons,

specifically - winter and summer period based on their average temperatures. The summer season is from May - October and the rest of the months are winter period.

The Table C.2 in Appendix C provides a summary of key weather variables, including maximum and minimum temperatures, humidity, and air pollutants (CO, NO2, NO, PM10, SO2, O3), during different periods, such as the entire year, winter season, and summer season. Overall, we observe significant differences in weather conditions between the winter and summer seasons. During the winter season, maximum and minimum temperatures are lower compared to the summer season, resulting in lower levels of humidity and air pollutants such as ozone (O3) and nitrogen dioxide (NO2). Conversely, during the summer season, we see higher temperatures, increased humidity levels, and elevated concentrations of air pollutants, particularly ozone and nitrogen dioxide. These findings highlight the importance of considering seasonal variations in weather conditions when analyzing cardiovascular health outcomes and planning public health interventions. For the monthly development of variables see Figure C.2 in Appendix C.

Lastly, to analyse the interdependencies among variables, we constructed a correlation plot (Figure 2.7) that visually represents the pairwise correlations. We can identify potential multicollinearity among predictors. Ozone levels exhibit a high positive correlation of 0.69 with temperature and a negative correlation of -0.72 with nitrogen dioxide (NO2). Additionally, nitrogen dioxide (NO2) shows a positive correlation of 0.67 with carbon monoxide (CO) and a correlation of 0.66 with temperature. Sulfur dioxide (SO2) correlates positively with carbon monoxide (CO) at 0.58.

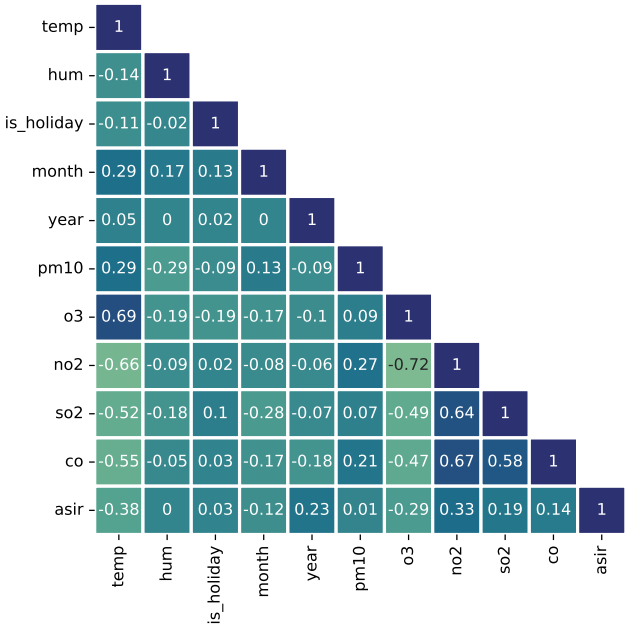

FIGURE 2.7: Correlation plot

Chapter 3

Methodology

3.1 ARIMA, SARIMA and SARIMAX Models

ARIMA, or Autoregressive Integrated Moving Average, is a widely used time series forecasting method that models the next step in the sequence as a linear function of the observations and their lagged values, trends, and stationarity through differencing. It combines autoregression (AR), differencing (I), and moving average (MA) components to capture the temporal dependencies and patterns present in the data. As described in book by Shumway and Stoffer, 2011, the following components are described as:

Autoregressive (AR) Component (p): The AR part of the model captures the relationship between an observation and a number of lagged observations (i.e., the series itself). It expresses the current value of the series as a linear function of its own past values, weighted by coefficients. The AR(p) model can be formulated as:

$$y_t = \phi_1 y_{t-1} + \phi_2 y_{t-2} + \ldots + \phi_p y_{t-p} + \epsilon_t$$

where $\phi_1, \phi_2, \ldots, \phi_p$ are the parameters of the model, and ϵ_t is the white noise error term at time t.

Integrated (I) Component (d): The I part of ARIMA involves differencing the time series data to achieve stationarity. Stationarity means that the statistical properties of the series, such as mean and variance, do not change over time. Differencing involves subtracting the previous observation from the current observation. For example, $\Delta y_t = y_t - y_{t-1}$ for first-order differencing. The parameter d represents the number of differencing steps needed to achieve stationarity.

Moving Average (MA) Component (q): The MA part of the model captures the relationship between an observation and a residual error from a moving average model applied to lagged observations. The MA(q) model can be expressed as:

$$y_t = \epsilon_t + \theta_1 \epsilon_{t-1} + \theta_2 \epsilon_{t-2} + \ldots + \theta_q \epsilon_{t-q}$$

where $\theta_1, \theta_2, \ldots, \theta_q$ are the parameters of the model, and ϵ_t is the white noise error term at time t.

Seasonal ARIMA (SARIMA) extends ARIMA to incorporate seasonal variations alongside non-seasonal components, addressing periodic patterns in the data.

Seasonal Autoregressive (SAR) Component (P): Models the relationship between an observation and its seasonal lagged observations.

The SAR(P) component is formulated as:

$$y_t = \phi_1^* y_{t-s} + \phi_2^* y_{t-2s} + \ldots + \phi_P^* y_{t-Ps} + \epsilon_t$$

where $\phi_1^*, \phi_2^*, \ldots, \phi_P^*$ are the seasonal AR parameters, and s is the seasonal period.

Seasonal Moving Average (SMA) Component (Q): Captures the dependency between an observation and its seasonal lagged forecast errors.

The SMA(Q) component is represented as:

$$y_t = \epsilon_t + \theta_1^* \epsilon_{t-s} + \theta_2^* \epsilon_{t-2s} + \ldots + \theta_Q^* \epsilon_{t-Qs}$$

where $\theta_1^*, \theta_2^*, \ldots, \theta_Q^*$ are the seasonal MA parameters.

Seasonal Differencing (D): Extends the non-seasonal differencing d to account for seasonal variations and achieve stationarity across seasonal cycles.

Seasonal differencing can be applied to the series y_t as:

$$\Delta_s y_t = y_t - y_{t-s}$$

where s is the seasonal period, and Δ_s denotes the seasonal differencing operator. The parameter D specifies the number of seasonal differencing steps needed.

SARIMAX extends SARIMA by incorporating exogenous variables (denoted as X_t) that are external to the time series but may influence it. Exogenous variables are additional factors that may impact the time series but are not influenced by it. These variables can improve the model's forecasting accuracy by accounting for external influences on the target variable.

Before including any exogenous variable, specifically environmental data, we closely looked at target variable. Starting by evaluating the stationarity of the time series data by performing the Augmented Dickey-Fuller (ADF) test to ensure the series is suitable for modelling. Furthemore, by plotting ACF and PACF (Figure 3.1) we can observe the temporal dependencies and seasonality. There is an annual seasonality present, specifically the ASIR increases during the winter months and is more subtle during the hot months and also that there are some statistically significant lagged values present.

Due to the data exhibiting seasonal patterns, ARIMA model may not be the best model, therefore we may consider SARIMA, which adds seasonal parameters to ARIMA model. Using the `pmdarima` library in Python, we employed an automated approach to determine the optimal SARIMA model parameters.

After fitting the SARIMA model, we evaluated its performance and diagnostic checks. Diagnostic plots, including residual analysis and model diagnostics such as Ljung-Box test for autocorrelation in residuals, were examined to ensure the model's adequacy. These visual and statistical tests verified that the SARIMA model captured the underlying patterns in the data effectively.

In order to evaluate if environmental variables can improve prediction accuracy, we explored the SARIMAX model. This extension allows for modeling additional factors that could impact the seasonal patterns observed in the time series.

In the context of time series analysis, the equation for a Seasonal Autoregressive Integrated Moving Average with Exogenous Variables (SARIMAX) model is given by:

FIGURE 3.1: ACF and PACF plots

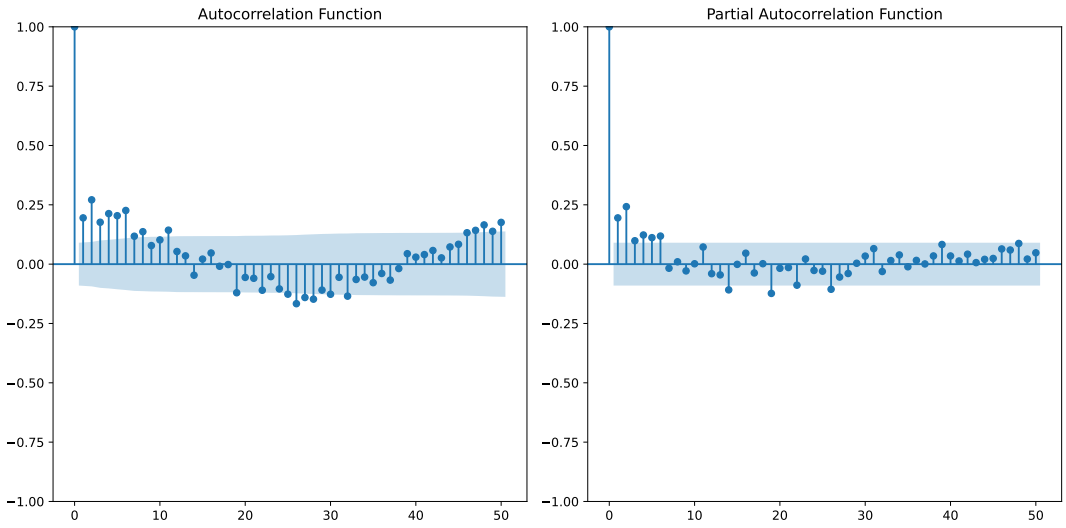

$$y_t = \phi_p y_{t-1} + \cdots + \phi_1 y_{t-p} + \theta_q \varepsilon_{t-q} + \cdots + \theta_1 \varepsilon_{t-1} + \varepsilon_t$$
$$+\theta_{s \cdot q} \varepsilon_{t-s \cdot q} + \cdots + \theta_s \varepsilon_{t-s} + \cdots + \beta_1 x_{1,t} + \cdots + \beta_k x_{k,t}$$

where:

- y_t represents the value of the time series at time t,
- $\phi_1, \phi_2, \ldots, \phi_p$ are the autoregressive (AR) parameters of the model representing the coefficients of past values of the series,
- p is the order of the autoregressive process,
- $\theta_1, \theta_2, \ldots, \theta_q$ are the moving average (MA) parameters of the model representing the coefficients of past errors,
- q is the order of the moving average process,
- ε_t denotes the error term or random shock at time t,
- s is the seasonal period,
- $\theta_{s \cdot q}, \theta_{s \cdot (q-1)}, \ldots, \theta_s$ are the seasonal moving average parameters,
- $\beta_1, \beta_2, \ldots, \beta_k$ are the coefficients of exogenous variables $x_{1,t}, x_{2,t}, \ldots, x_{k,t}$.

3.2 The Recurrent Neural Network

In the field of deep learning, Recurrent Neural Networks (RNN) are defined as artificial neural networks that are bi-directional. As being part of a supervised learning their usage is universal and also multidisciplinary. They are commonly used for time-series data analysis and forecasting, classification, regression, image/video processing and many other problems. The main concept of the RNN is that the neural network is based on cycles meaning that the network depends not only on the current data but also on the previous data it used (Hrnjica and Bonacci, 2019). In

other words, the output from nodes can have an affect on other input provided to the same nodes. Figure 3.2 shows an example of a single RNN cell. The hidden state is looped back and used on other input. The main setbacks of RNN are that they are computationally very costly, meaning they are slow. Furthermore, they can only carry short-term information and lastly, they tend to have vanish gradient problem (when change in gradient is close to 0 or very small) implying that the model stops learning.

FIGURE 3.2: A single RNN Cell

Source: Olah, 2015

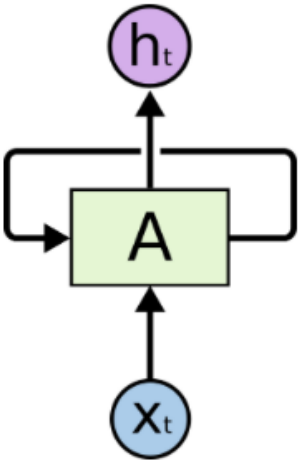

To overcome most of the problems, Long Short-Term Memory networks (LSTM), are a special kind of RNN, that were designed. LSTM has an extra cell state added. The networks are able to keep information over long sequences and can overcome the vanishing gradient problem. When it comes to the architecture of LSTM, has a chain like structure, as a network it has a special design. It contains only four neural networks and different memory cells, that regulate flow of information. Each contain three main components - input, forget and output gates, which are multiplicative units that help to store, update and retrieve information over long sequences. As described in Peixeiro, 2022, the structure of an LSTM cells is as follows.

3.2.1 Structure of an LSTM Cell

- *Cell State (C_t):*

  The cell state is a key feature of LSTMs, allowing information to be carried across long sequences. It acts as a memory that can maintain relevant information throughout the processing of sequences. Furthermore, the cell state is updated with the help of the forget and input gates, which are both described below. For now, it is important to note that both gates contain weights that help to decide which time-steps to incorporate into the cell state. They are not all equally incorporated which makes LSTM interesting in their ability to dynamically and adaptively decide what periods to include.

- *Hidden State (h_t):*

The hidden state contains the output of the LSTM cell at each time step. It is also passed to the next cell and is used to compute the output of the network. In other words, it can be seen as an encoding of the latest time-step.

- *Forget Gate (f_t):*

  The forget gate decides which information from the cell state should be discarded. It takes the previous hidden state (h_{t-1}) and the current input (x_t). It is further multiplied by the weight matrices and additional bias. The output is a number between 0 and 1 for each number in the cell state C_{t-1}. Outputs close to 0 mean that the information is forgotten and close to 1 the information retains and is very important.

  Mathematically, $f_t = \sigma(W_f \cdot [h_{t-1}, x_t] + b_f)$, where σ is the sigmoid activation function, W_f are the weights, and b_f is the bias.

- *Input Gate (i_t):*

  The input gate determines which new information will be stored in the cell state. It consists of two parts: an update vector ($\tilde{C}_t$) and the gate itself. The sigmoid function regulates and filters information with the use of inputs h_{t-1} and x_t.

  The gate, i_t, is calculated similarly to the forget gate: $i_t = \sigma(W_i \cdot [h_{t-1}, x_t] + b_i)$.

  The update vector, $\tilde{C}_t$, uses the activation *tanh* function which output ranges between -1 and 1 containing all possible values of h_{t-1} and x_t. Then the values of the vector and the regulated values are multiplied to create a vector of new candidate values: $\tilde{C}_t = \tanh(W_C \cdot [h_{t-1}, x_t] + b_C)$.

- *Cell State Update:*

  The cell state is updated by combining the old cell state and the new candidate values. The forget gate f_t controls what proportion of the old cell state should be kept, and the input gate i_t controls how much of the candidate values should be added.

  Mathematically, $C_t = f_t * C_{t-1} + i_t * \tilde{C}_t$.

- *Output Gate (o_t):*

  The output gate determines the next hidden state, which will be used in the next time step and as the output of the current time step. It combines the previous hidden state and the current input to decide which parts of the cell state will be output. In other words, we generate a vector by applying *tanh* function and regulate and filter the information using sigmoid function, inputs h_{t-1} and x_t. One of the functions of *tanh* function is to normalise encoding of the data.

  The output gate is calculated as: $o_t = \sigma(W_o \cdot [h_{t-1}, x_t] + b_o)$.

  The new hidden state h_t is then calculated as: $h_t = o_t * \tanh(C_t)$.

3.2.2 Working Mechanism

At each time step, the LSTM cell takes in the current input x_t and the previous hidden state h_{t-1}. The forget gate determines which parts of the previous cell state C_{t-1} should be retained. The input gate decides which new information from the current input x_t should be added to the cell state. The cell state is then updated accordingly. Finally, the output gate computes the new hidden state h_t, which serves as the output for the current time step and will be passed to the next LSTM cell.

LSTM cells, with their unique gating mechanisms, provide a powerful way to capture long-term dependencies and temporal patterns in time series data. By carefully controlling the flow of information through forget, input, and output gates, LSTMs effectively address the limitations of traditional RNNs, making them suitable for complex predictive modeling tasks.

FIGURE 3.3: A single LSTM Cell

Source: Olah, 2015

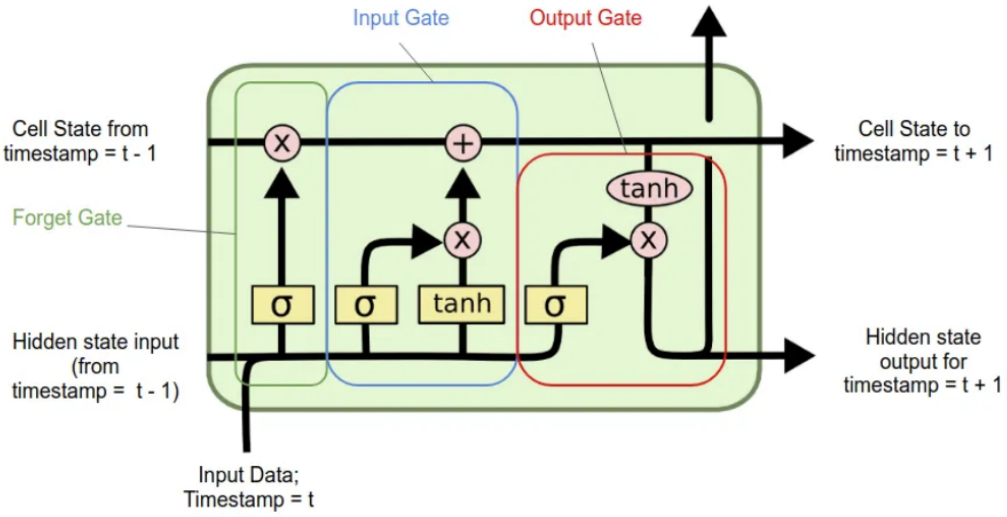

Recurrent Neural Networks (RNN) with Long Short-Term Memory (LSTM) units to predict the incidence of AMI based on environmental factors. RNN-LSTM is chosen for its capability to model time series data with complex temporal dependencies and non-linear relationships thanks to LSTMs feedback connections.

3.2.3 LSTM in practice

Prior to training the models, there has been data preprocessing involved so the data would be suitable for LSTM. Normalization was performed using MinMaxScaler to scale the feature variables to a range of 0 to 1. The target variable, representing ASIR, was similarly scaled.

To prepare the data for the LSTM model, the time series data was converted into sequences. This involved creating fixed-length sequences of input features and corresponding target values. A sequence length of 12 days was chosen based on domain knowledge and preliminary experiments.

The data was divided into training and testing sets, with around 85% of the data allocated for training and the remaining 15% for testing, more specifically train set

was years 2010-2017 and test set was year 2018. This split ensured that the model had sufficient data for training while still providing a robust test set for evaluation.

3.2.4 Hyperparameters optimisation

Hyperparameter optimisation (also called hyperparameter tuning) is a process of selecting the optimal configuration of model hyperparameter values such that the model performance is optimised with respect to some performance metric (Wu et al., 2019). Unlike model parameters, which are estimated from the data, model hyperparameters cannot be estimated from the data, and their values are selected prior to model training. A few common methods of performing hyperparameter optimisation include Random Search, Bayesian optimisation, and Sequential Model-Based Optimization (SMBO),the last one uses a surrogate model to iteratively explore the hyperparameter space and find the configuration that maximizes the model's performance.

Random search is a search algorithm that iterates over some pre-specified number n of combinations of hyperparameter values to find the optimal setting (De Sa, 2020). First, a distribution of values is defined for every hyperparameter being optimised, and then n combinations of hyperparameter values are sampled randomly from the joint distribution of the hyperparameter values. For each of these n settings, a model is fit and evaluated. The best setting is the one that minimises the metric of interest the most, i.e. results in the smallest loss. In random search, the combinations of hyperparameter settings at each iteration are independent.

This is not the case for Bayesian optimisation (Brochu, Cora, and De Freitas, 2010). Bayesian optimisation is an optimisation strategy that performs an 'informed' search through the parameter space, in the sense that it incorporates knowledge about previous combinations to sample the next combination. It aims to find the extrema of a function – in the context of hyperparameter optimisation, the objective of Bayesian optimisation is to find a minimum of the loss function. The algorithm starts by specifying the probability distributions of the hyperparameter values, and sampling multiple points from the joint distribution of the hyperparameter values. Then, a surrogate function (which is an approximation of the loss function that can be expressed as a probability distribution) is formed based on the sampled points. The algorithm then identifies the next combination of hyperparameter values such that it compromises between searching previously unexplored areas of the surrogate function with high uncertainty, and areas which lead to further improvement of the surrogate function. The surrogate function then gets updated by making use of Bayes Theorem, which is given by:

$$P(f \mid \mathcal{D}) \propto P(\mathcal{D} \mid f)P(f),$$

where the prior distribution (the surrogate function) $P(f)$ is multiplied by the likelihood function $P(\mathcal{D} \mid f)$, and $P(f \mid \mathcal{D})$ represents the resulting posterior distribution.

The parameters that can be tuned in an LSTM include:

Number of units in each LSTM layer: This determines the dimensionality of the output space. More units can capture more complex patterns but might lead to overfitting.

Number of LSTM layers: Multiple layers can capture hierarchical patterns in the data, but adding too many layers can make the model unnecessarily complex.

Dropout rate: Dropout is a regularization technique used to prevent overfitting by randomly setting a fraction of input units to 0 at each update during training. A higher dropout rate means more units are dropped, leading to stronger regularization.

Learning rate: This controls how much the model is adjusted in response to the estimated error each time the model weights are updated. A lower learning rate means the model learns more slowly but can converge to a better solution.

Batch size: The number of samples processed before the model is updated. Smaller batch sizes can lead to more stable learning but can be computationally expensive.

Activation function: Determines the output of a node. Common choices for LSTM include tanh and ReLU.

Optimizer: The algorithm used to change the attributes of the neural network such as weights and learning rate in order to reduce the losses. Common optimisers include Adam, RMSprop, and SGD.

Chapter 4

Results

4.1 Model Comparison and Results

4.1.1 SARIMA/SARIMAX Model Results Summary

The SARIMAX model has successfully converged, indicating a stable optimization process. The optimal model suggested was specified as SARIMAX(1, 1, 1)x(2, 0, 0, 52), indicating one autoregressive term, one differencing term, one moving average term, and two seasonal autoregressive terms with an annual periodicity of 52 weeks.

We constructed models with and without exogenous variables and plotted the predictions in Figure 4.1. It can be observed that the SARIMAX model, which incorporates exogenous variables, demonstrates better performance when it comes to capturing dynamic changes, especially sudden drops and increases throughout the year. This model exhibits less smoothness and closely follows the observed trend, highlighting its ability to incorporate external factors effectively. Furthermore, our selection of exogenous variables suggests that environmental factors indeed correlate with ASIR fluctuations and captures additional sources of variability. Specifically, SARIMA exhibits a delayed response to these fluctuations causing predictions being shifted to the right.

The performance comparison between the SARIMA and SARIMAX models is summarized in Table 4.1. The SARIMAX model outperforms the SARIMA model in both training and validation datasets. Specifically, the SARIMAX model achieved a Training MAE of 0.148 compared to 0.158 for the SARIMA model, and a Validation MAE of 0.151 compared to 0.184 for the SARIMA model. Similarly, the Training MAPE for the SARIMAX model was 15.7% compared to 16.7% for the SARIMA model, and the Validation MAPE was 15.2% compared to 19.9% for the SARIMA model. These results clearly demonstrate that incorporating exogenous variables significantly improves the model's accuracy.

TABLE 4.1: Performance Comparison between SARIMA and SARIMAX Models

	Train		Test	
Model	MAE	MAPE (%)	MAE	MAPE (%)
SARIMA	0.158	16.7	0.184	19.9
SARIMAX	**0.148**	**15.7**	**0.151**	**15.2**

This table highlights the improvements made by the SARIMAX model in both training and validation phases, emphasizing the importance of incorporating exogenous variables for better predictive performance.

FIGURE 4.1: SARIMA vs SARIMAX predictions

(A) Time Series Fitted by SARIMA

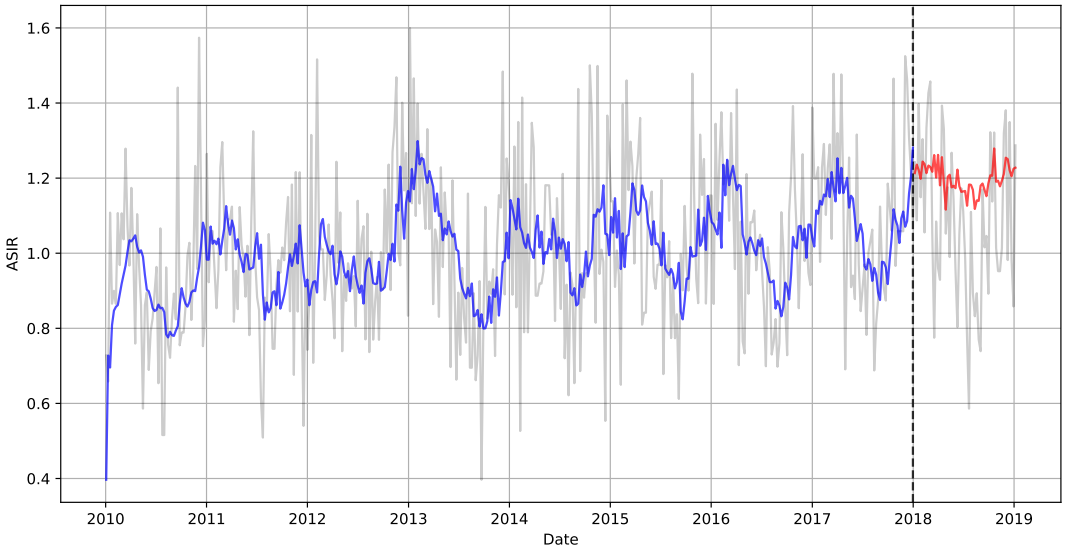

(B) Time Series Fitted by SARIMAX

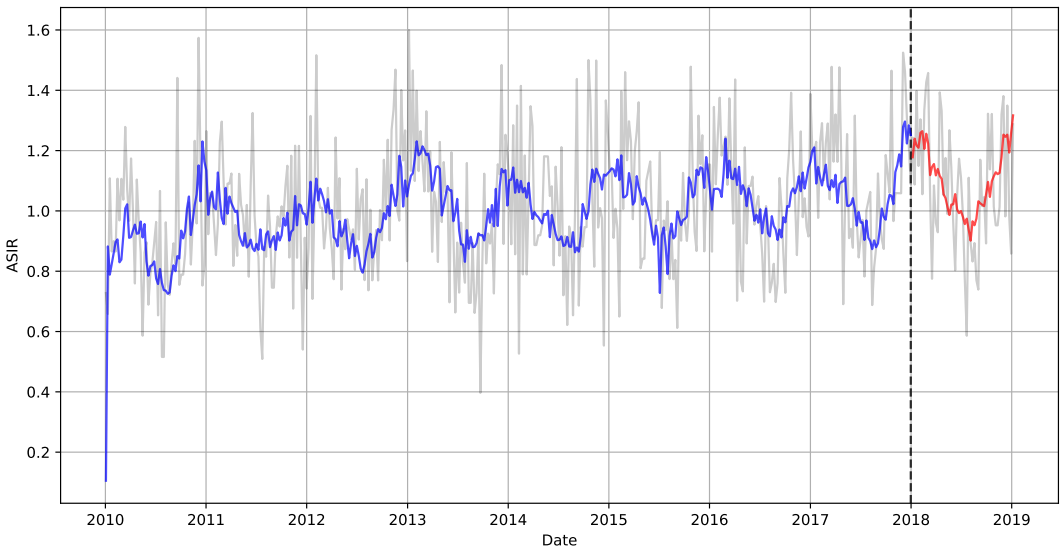

Moreover, we conducted a parameter tuning process for the SARIMAX model using a grid search approach. This involved evaluating multiple combinations of parameters through cross-validation, aiming to identify the optimal set that maximizes the model's predictive performance. Using TimeSeriesSplit cross-validation and tracking performance metrics, such as mean squared error (MSE), across different parameter configurations, we identified and selected the most suitable SARIMAX model for forecasting.

4.1.2 LSTM Model Results Summary

Keras Tuner, which is frequently used to find optimal parameters for a neural networks (O'Malley et al., 2019), was utilized to optimize the hyperparameters of the LSTM model.The following hyperparameters were determined using Keras Tuner, which involved a random search over the specified hyperparameter space. The search process used a maximum of 30 trials, with each trial executed 3 times to ensure robustness in the evaluation. Early stopping was employed during training to prevent overfitting and to restore the best weights based on validation loss.

Best Hyperparameters and Model Description

The hyperparameter optimisation process identified the following optimal hyperparameters for the LSTM model and together with the model is described below:

TABLE 4.2: Model Architecture

```
Model: "sequential"
_________________________________________________________________
 Layer (type)                Output Shape              Param #
=================================================================
 input_1 (InputLayer)        [(30, 8)]                 0

 lstm_1 (LSTM)               (200,)                    167200

 dropout_1 (Dropout: 0.2)    (200,)                    0

 dense_1 (Dense)             (1,)                      201
=================================================================
Total params: 167401
Trainable params: 167401
Non-trainable params: 0
_________________________________________________________________

Optimizer: Adam
Activation Function: ReLU
```

The model was compiled with the Adam optimizer and mean squared error as the loss function. The training configuration included:

Epochs: 100

Batch size: 32

Validation split: 0.1

Model Training

The training process was monitored using a validation split of 10%, and early stopping was applied with a patience of 10 epochs. The early stopping mechanism monitored the validation loss, with a minimum delta of 0.01 for improvements to be considered significant.

The final model, trained with the best hyperparameters, exhibited robust performance with the specified architecture and training configuration. The use of dropout layers helped in mitigating overfitting, and the choice of the Adam optimizer ensured efficient and effective convergence of the model parameters.

The LSTM model with incorporating exogenous variables performs very similarly to SARIMAX model. Table 4.3 displays the evaluation metrics in LSTM model for both training and testing period. The predictions are visually presented in Figure 4.2.

FIGURE 4.2: LSTM predictions with exogenous variables

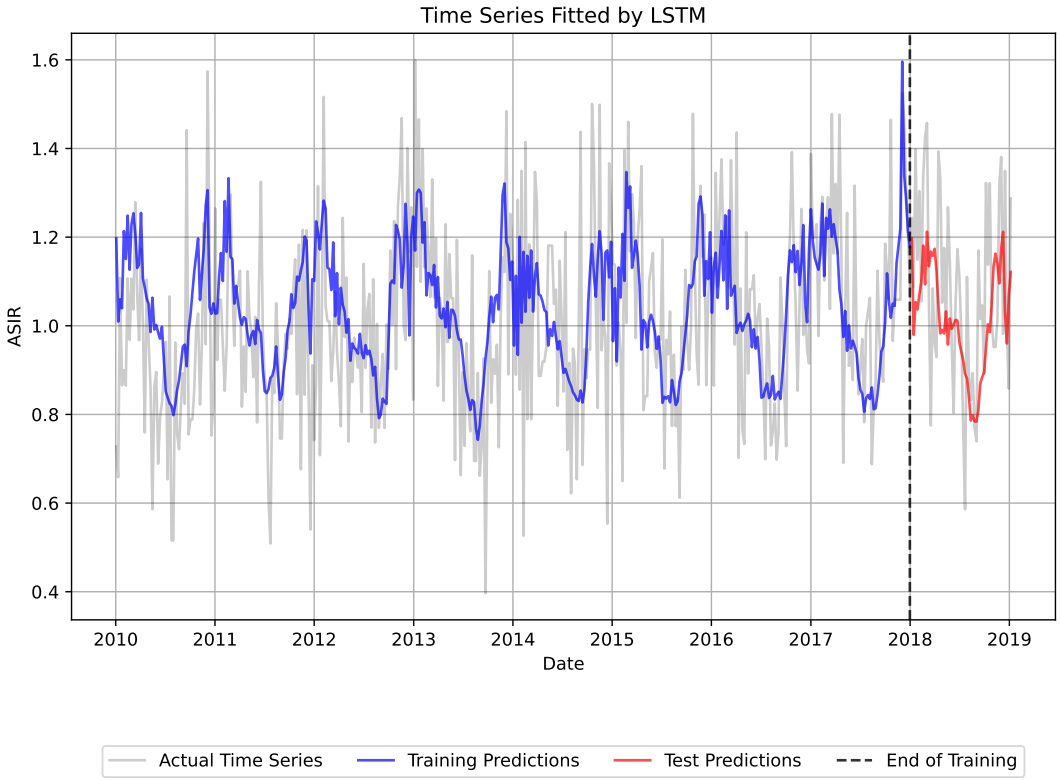

TABLE 4.3: Evaluation metrics for LSTM (Exogenous Variables)

Metric	Train	Test
MAE	0.156	0.159
MSE	0.039	0.041
RMSE	0.203	0.203
MAPE	16.93%	15.69%

4.2 Feature Importance

Feature importance is a technique that is used to obtain the impact of variables on model predictions. There are various methods that extract and analyse the importance such as permutation feature importance, feature importance from model coefficient, Shapley Additive Explanations (SHAP) values or Local Interpretable Model-agnostic Explanations (LIME). In this analysis, we are going to take a closer look at the first two methods.

4.2.1 Permutation Feature Importance

The permutation feature importance is a method that measure the importance of the feature by comparing the error of the model with and without permuting the feature's values. A feature is considered important if the model error increases after the values are permuted suggesting the reliance of the model on the feature Molnar (2022).

In our case, the analysis aims to understand the contribution of individual environmental variables—temperature, humidity, and pollution—to the predictive performance of the LSTM model with exogenous variables. The model's ability to capture and utilise these features is crucial for interpreting its predictions. Together with the feature importance we can improve the understanding of a "black box" prediction model.

We assessed the importance of each feature by evaluating the mean absolute error (MAE) when each feature was individually shuffled while keeping others unchanged. There are also other techniques that could be used such as added noise, integrated gradients or ablation Freeborough and Zyl (2022). This method allows us to quantify the impact of each feature on the accuracy of the model's predictions. The results of this analysis are summarized in Table 4.4. To ensure robustness in our feature importance analysis, we employed K-fold cross-validation. This method involves splitting the dataset into K folds, training the model on K-1 folds, and validating it on the remaining fold. We repeated this process K times, each time with a different validation fold, to obtain a comprehensive assessment of the model's performance.

Figure 4.3 illustrates the outcomes of the feature importance analysis, visually depicting the MAE values associated with each environmental variable. These findings highlight the relative importance of temperature, humidity, and various pollutants in influencing the model's predictive performance. We can observe the among the evaluated features, MAE of temperature is the highest value, i.e. 0.18, which indicates it to be the highest of importance. As the second most important variable is humidity with MAE = 0.169. The pollutants have approximately the same importance around 0.163.

TABLE 4.4: Feature Importance based on Mean Absolute Error (MAE)

Feature	MAE	% Increase
Baseline MAE	*0.1590*	–
Temperature	0.1800	13.21%
Humidity	0.1689	6.23%
SO2	0.1640	3.14%
NO2	0.1635	2.83%
CO	0.1629	2.45%
PM10	0.1624	2.14%

FIGURE 4.3: Feature Importance in LSTM Model with Exogenous Variables

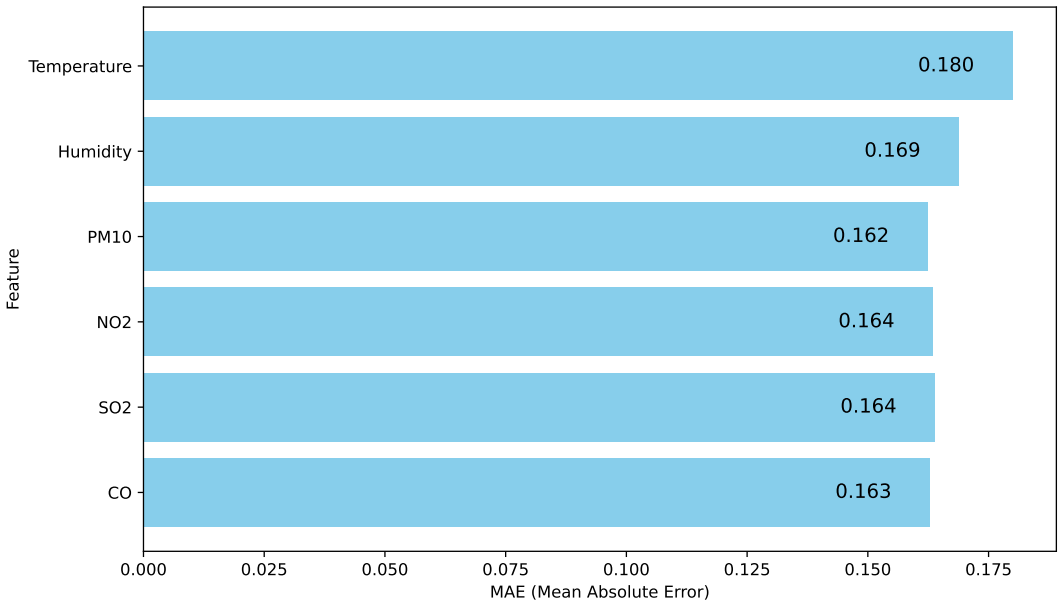

From the analysis, we observe that temperature exhibits the highest influence on AMI incidence predictions, followed by humidity and pollution levels. These findings suggest that temperature fluctuations play a significant role in the occurrence of AMI, aligning with previous research highlighting the impact of weather on cardiovascular health.

4.2.2 Feature Importance from Model Coefficients

Another commonly used method involves assessing feature importance based on model coefficients, particularly in linear models, where higher magnitude coefficients indicate more significant contributions to predictions. It is important to note that these coefficients represent linear dependencies within the SARIMAX framework.

We observe that temperature exhibits the largest negative coefficient magnitude (-0.362), indicating a strong negative relationship with AMI incidence predictions in the SARIMAX model. Higher temperatures are associated with lower predicted

AMI incidence, aligning with established physiological effects of heat on cardiovascular health. In contrast, humidity (coefficient -0.068) shows a smaller effect size, suggesting a weaker impact on AMI incidence in this model context. The presence of pollutants such as PM10 (coefficient 0.153) and NO2 (coefficient 0.1632) also demonstrates significant coefficients, albeit with positive signs indicating potential positive associations with AMI risk.

4.3 Prediction skill vs Lead-time

An important issue to explore in this context is the prediction skill versus lead-time. While the current approach predicts the entire validation period of one year as a whole, in practice, an Early Warning System (EWS) would be continuously updated as new data becomes available. Therefore, it is crucial to assess whether there is a degradation in the performance of the models as the lead-time increases. This is particularly relevant since the models rely on both forecasts of the target variable and the exogenous variables.

To investigate this, we can compare the prediction skill at different lead-times, ensuring that the forecasts are updated continuously using the most recent observations. Specifically, we can measure the model's performance at various points within the validation period, examining how the accuracy of predictions changes as the forecast horizon extends.

We implemented a rolling forecast approach, where the model is updated with new data and forecasts are made for lead-times ranging from 1 to 50 weeks. The performance of the model was evaluated using Mean Absolute Error (MAE) and Mean Absolute Percentage Error (MAPE) for these different lead-times. The results in Table 4.5 show how the prediction accuracy degrades as the lead-time increases, which is crucial for understanding the reliability of the EWS over extended forecast horizons.

TABLE 4.5: Prediction Skill vs Lead Time

Lead Time	MAE	MAPE (%)
1	0.1549	15.34
15	0.1453	14.92
20	0.1466	15.56
25	0.1548	16.56
30	0.1456	14.53
35	0.1620	15.04
40	0.1758	16.63
45	0.1902	18.11
50	0.2141	23.21

We observe that the model achieves relatively accurate forecasts for shorter lead-times, such as 1 week, with a Mean Absolute Error (MAE) of approximately 0.155 and a Mean Absolute Percentage Error (MAPE) of about 15.34%. However, as the lead-time extends, we observe a decline in prediction accuracy. For instance, at a lead-time of 25 weeks, the MAE increases to around 0.155 and the MAPE rises to 16.56%. This trend continues, with the MAE and MAPE reaching 0.214 and 23.21%, respectively, at a lead-time of 50 weeks. For graphical visualisation see Figure 4.4. These findings highlight that in order to maintain prediction accuracy over longer

forecast, it is important to update the model and add new data regularly to maintain the accuracy and effectiveness of the EWS.

FIGURE 4.4: Prediction Skill vs Lead-time

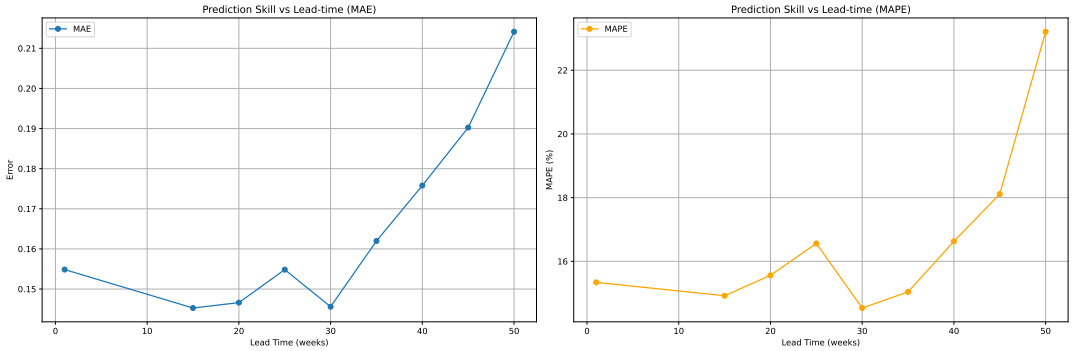

4.4 Limitations

The SARIMAX model, while useful for modeling time series data, has several limitations. Firstly, it assumes linear relationships between the predictor variables and the response variable. However, this may not accurately capture the complex nonlinear relationships that exist in the data. Additionally, SARIMAX models are sensitive to outliers and extreme values, which can lead to biased estimates if not appropriately addressed. Moreover, the chosen seasonal and non-seasonal orders may not fully capture the seasonal patterns and trends present in the data, potentially resulting in model misspecification. Furthermore, SARIMAX models rely on the assumption of stationarity, which may not hold true for all time series data, further impacting model performance. Finally, SARIMAX models require accurate values of exogenous variables for prediction, and any inaccuracies in these variables can affect the accuracy of the forecasts.

Similarly, LSTM models have their own set of limitations. One major limitation is the requirement for a large amount of data for effective training. Without sufficient data, LSTM models may struggle to learn complex patterns and may suffer from poor performance. Additionally, hyperparameter tuning for LSTM models can be computationally intensive and may require extensive experimentation to identify optimal configurations. Furthermore, LSTM models are prone to overfitting, especially when trained on noisy or high-dimensional data, which can lead to poor generalization to unseen data. Lastly, the interpretability of LSTM models can be challenging due to their black-box nature, making it difficult to understand the underlying mechanisms driving predictions. Similar to SARIMAX models, LSTM models also require accurate values of exogenous variables for prediction, and any inaccuracies in these variables can impact the accuracy of the forecasts. What is more, to predict accurately the models using exogenous variables, there is also need to know those values for forecasting which makes it one of the crucial limitations of both models.

Furthermore, in our analysis, we utilized linear interpolation to derive daily estimates of population data from six-month county-level estimates. This approach ensured comprehensibility of the dataset, however it also introduces potential minor disruptions. Although these shifts are generally minimal due to the gradual

nature of population changes from year to year, they could still influence model performance.

Chapter 5

Conclusion and future directions

5.1 Conclusion

In summary, this study aimed to investigate the relationship between environmental factors and the incidence of AMI in Catalonia, Spain, through the lens of time series analysis. Encompassing hospital admissions, meteorological, and pollution data, we employed distinct modeling approaches: SARIMA, SARIMAX and LSTM.

Our results demonstrated that the SARIMAX model significantly outperformed the SARIMA model by incorporating exogenous variables, highlighting the importance of external factors in improving forecast accuracy. Furthermore, when assessing prediction skill versus lead-time, the SARIMAX model maintained superior performance, even as the forecast horizon extended.

Despite the promising results, the SARIMAX model has several limitations. It assumes linear relationships between predictor and response variables, which may not fully capture the complex nonlinear relationships in the data. Additionally, SARIMAX models are sensitive to outliers and extreme values, potentially leading to biased estimates. The model's reliance on accurate exogenous variable values for prediction poses a significant limitation, as inaccuracies in these variables can adversely affect forecast accuracy. The chosen seasonal and non-seasonal orders might also not fully capture all the seasonal patterns and trends, leading to model misspecification. Moreover, SARIMAX models assume stationarity, which may not hold true for all time series data, further impacting model performance.

The LSTM model, also has its limitations. It requires a large amount of data for effective training and is prone to overfitting, especially with noisy or high-dimensional data. Hyperparameter tuning for LSTM models is computationally intensive and requires extensive experimentation. The interpretability of LSTM models is challenging due to their black-box nature, making it difficult to understand the mechanisms driving predictions. Similar to SARIMAX, LSTM models require accurate values of exogenous variables for prediction, with any inaccuracies potentially impacting forecast accuracy.

5.2 Future Directions

Future research could explore several avenues to address the limitations identified in this study and further improve the predictive performance of time series models. One potential direction is to develop or integrate models that can capture complex nonlinear relationships between predictor and response variables, such as generalized additive models (GAMs) or machine learning approaches like random forests and gradient boosting. Implementing robust statistical methods to handle outliers

and extreme values, such as robust regression or outlier detection and treatment methods, could mitigate their impact on model performance.

Future studies could incorporate additional variables, such as socioeconomic factors, and lifestyle variables, to improve the predictive accuracy and robustness of the models. Enhancing the accuracy and reliability of exogenous variable forecasts could also improve the overall model performance. Moreover, advanced modeling techniques, including hybrid models that combine SARIMAX and LSTM, or other deep learning architectures such as Transformer models, could be explored to capture complex temporal dependencies and enhance prediction performance. Conducting a spatial analysis of AMI incidences to identify geographical hotspots and understand regional variations in the impact of environmental factors could also be beneficial.

Additionally, future research could leverage ERA5 data for grid-level temperature and relative humidity to improve the granularity and precision of the environmental variables used in the models. Incorporating this high-resolution climate data could enhance the understanding of how microclimate variations influence AMI incidences and improve the predictive accuracy of the models.

Appendix A

Code

The code of this project is available in the following link: Master Project GitHub repository.

Appendix B

Map of Catalonia split by Regions

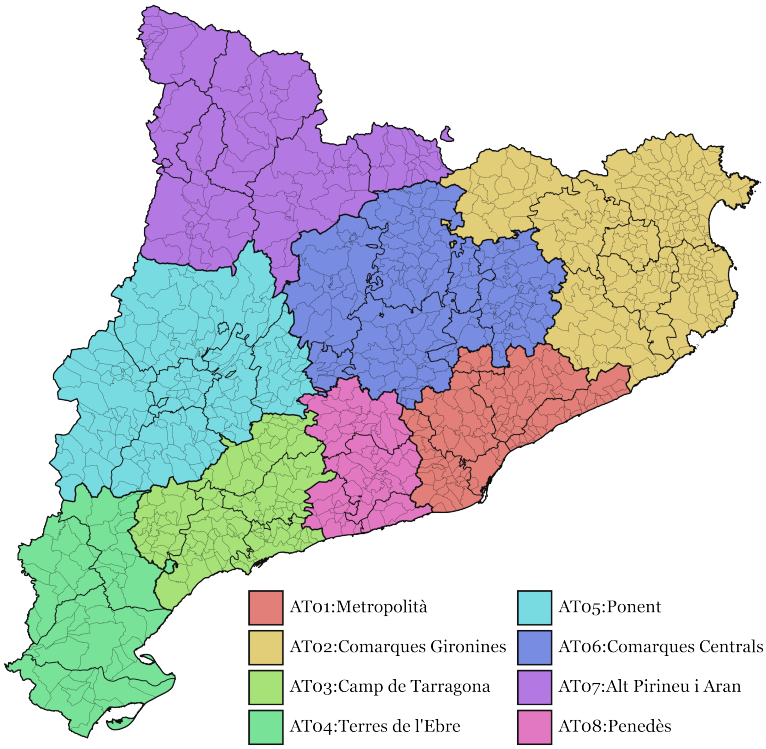

FIGURE B.1: Map of Catalonia split by Regions

Appendix C

Descriptive Statistics

FIGURE C.1: Decomposition of ASIR

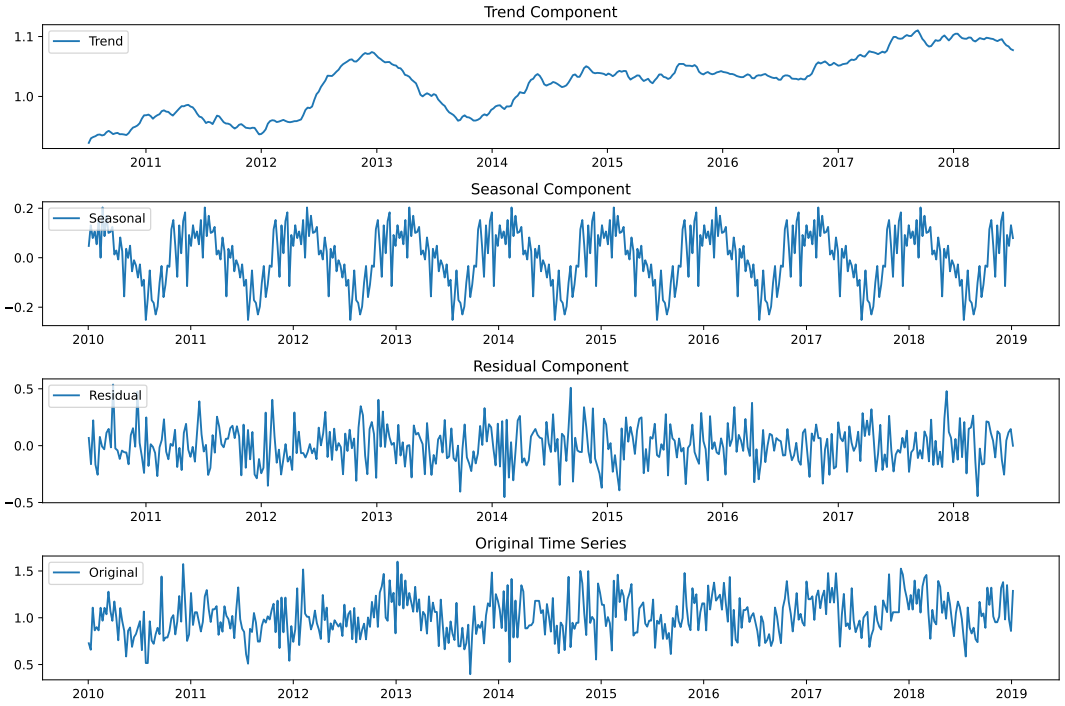

TABLE C.1: Age and Sex-Specific Trends in AMI Incidence with Statistical Significance

Age	Sex	Trend	T (0.025)	T (0.975)	R2	p-value	SE
20-24	Female	-0.033	-0.163	0.097	0.049	0.567	0.055
	Male	-0.063	-0.180	0.054	0.187	0.245	0.050
25-29	Female	-0.057	-0.180	0.066	0.146	0.310	0.052
	Male	0.059	-0.293	0.411	0.022	0.704	0.149
30-34	Female	-0.047	-0.182	0.087	0.091	0.431	0.057
	Male	0.323	-0.185	0.832	0.244	0.176	0.215
35-39	Female	0.125	-0.447	0.697	0.037	0.621	0.242
	Male	0.439	-0.259	1.137	0.240	0.180	0.295
40-44	Female	0.004	-0.456	0.463	0.000	0.985	0.194
	Male	0.031	-0.610	0.672	0.002	0.912	0.271
45-49	Female	0.316	-0.361	0.993	0.148	0.306	0.286
	Male	1.147	-0.145	2.439	0.386	0.074	0.546
50-54	Female	0.500	-0.296	1.297	0.240	0.181	0.337
	Male	**3.770**	**1.052**	**6.488**	**0.606**	**0.013**	**1.149**
55-59	**Female**	**1.237**	**0.551**	**1.922**	**0.722**	**0.004**	**0.290**
	Male	**4.408**	**1.087**	**7.729**	**0.585**	**0.016**	**1.404**
60-64	**Female**	**1.525**	**0.752**	**2.298**	**0.757**	**0.002**	**0.327**
	Male	**4.698**	**1.955**	**7.441**	**0.701**	**0.005**	**1.160**
65-69	**Female**	**1.156**	**-0.001**	**2.313**	**0.444**	**0.050**	**0.489**
	Male	2.760	-0.164	5.685	0.416	0.061	1.237
70-74	Female	0.160	-1.386	1.706	0.008	0.814	0.654
	Male	2.676	-0.707	6.058	0.333	0.104	1.431
75-79	Female	0.600	-2.114	3.315	0.038	0.617	1.148
	Male	**7.172**	**2.852**	**11.492**	**0.688**	**0.006**	**1.827**
80-84	Female	1.720	-0.539	3.980	0.317	0.115	0.955
	Male	**5.457**	**0.616**	**10.298**	**0.504**	**0.032**	**2.047**
85-89	**Female**	**3.734**	**0.830**	**6.639**	**0.569**	**0.019**	**1.228**
	Male	**4.006**	**0.461**	**7.550**	**0.505**	**0.032**	**1.499**
90-94	Female	1.512	-0.138	3.162	0.401	0.067	0.698
	Male	**4.919**	**0.753**	**9.084**	**0.527**	**0.027**	**1.762**
95+	Female	3.004	-0.823	6.831	0.330	0.106	1.618
	Male	5.388	-0.161	10.937	0.430	0.055	2.347

FIGURE C.2: Development of variables over years for Catalonia on monthly basis

(A) Maximum Relative Humidity

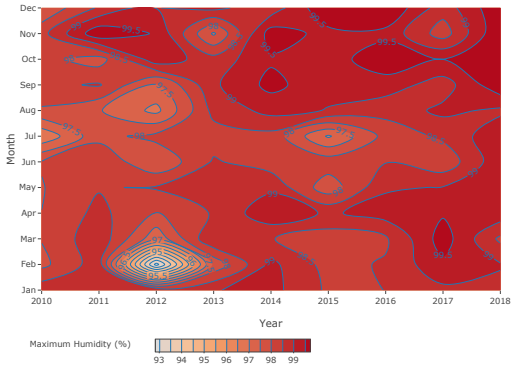

(B) Minimum Relative Humidity

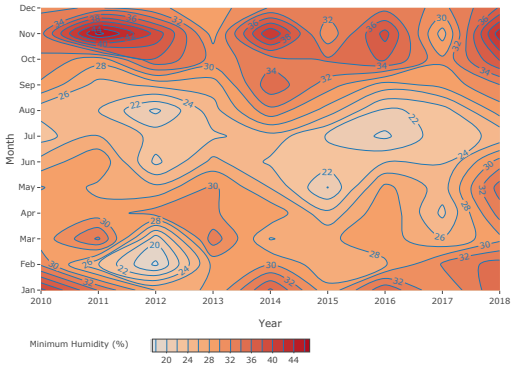

(C) Maximum Temperature

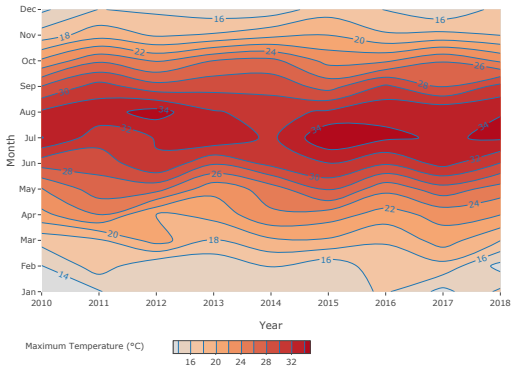

(D) Minimum Temperature

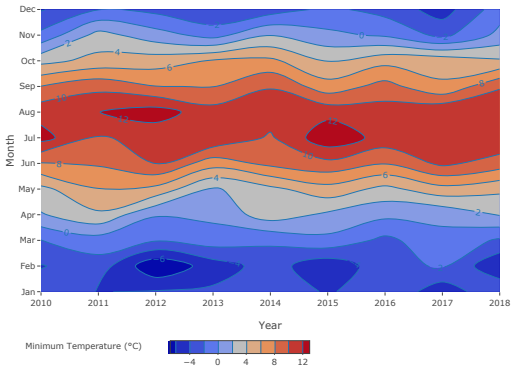

(E) Maximum Ozone

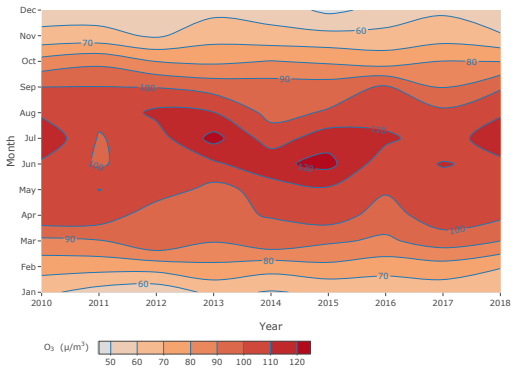

(F) Maximum PM10

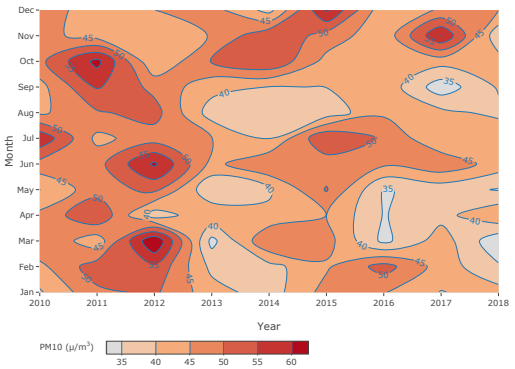

TABLE C.2: Descriptive statistics for daily levels of meteorological variables and air pollutant levels (Lag0) in Catalonia.

Variable	Mean	SD	Minimum	Q25	Median	Q75	Maximum	IQR
All - 3287 days								
Max Temperature	23.50	7.51	1.70	17.40	23.20	29.70	43.00	12.30
Min Temperature	3.30	7.03	-23.20	-1.80	3.10	8.70	20.70	10.50
Max Humidity	98.63	3.08	62.00	99.00	100.00	100.00	100.00	1.00
Min Humidity	29.23	13.66	0.00	20.00	28.00	37.00	89.00	17.00
Max CO	0.52	0.28	0.13	0.32	0.45	0.62	4.60	0.30
Max NO2	50.13	19.41	6.20	35.91	48.50	62.42	222.00	26.50
Max NO	43.37	39.66	1.00	14.10	31.46	60.19	531.00	46.09
Max PM10	44.60	22.29	4.00	31.50	40.75	52.55	658.00	21.05
Max SO2	5.94	5.52	0.67	3.00	4.50	7.00	110.80	4.00
Max O3	87.96	24.51	17.75	70.29	88.67	104.83	184.00	34.55
Winter - 1631 days								
Max Temperature	17.53	4.41	1.70	14.60	17.50	20.40	34.90	5.80
Min Temperature	-1.71	4.89	-23.20	-4.60	-1.40	1.60	12.70	6.20
Max Humidity	98.70	3.21	62.00	99.00	100.00	100.00	100.00	1.00
Min Humidity	31.14	15.33	0.00	20.00	30.00	41.00	89.00	21.00
Max CO	0.60	0.31	0.13	0.40	0.54	0.73	4.60	0.33
Max NO2	56.81	19.27	6.50	43.62	56.20	69.00	165.00	25.38
Max NO	59.37	45.81	1.20	23.54	49.26	84.90	531.00	61.36
Max PM10	44.50	21.05	4.00	30.71	41.00	53.67	317.50	22.95
Max SO2	6.64	5.22	0.67	3.50	5.18	8.00	89.29	4.50
Max O3	74.45	21.42	17.75	58.67	72.80	89.71	152.00	31.05
Summer - 1656 days								
Max Temperature	29.34	4.84	7.40	26.00	29.60	33.00	43.00	7.00
Min Temperature	8.21	5.08	-14.40	5.00	8.60	12.00	20.70	7.00
Max Humidity	98.55	2.95	71.00	98.00	100.00	100.00	100.00	2.00
Min Humidity	27.35	11.50	1.00	19.00	26.00	34.00	81.00	15.00
Max CO	0.43	0.22	0.13	0.30	0.40	0.50	2.90	0.20
Max NO2	43.59	17.19	6.20	31.29	41.74	53.36	222.00	22.08
Max NO	27.68	23.70	1.00	10.09	21.00	38.45	214.00	28.36
Max PM10	44.70	23.44	6.00	32.00	40.50	51.50	658.00	19.50
Max SO2	5.26	5.73	0.67	2.67	3.83	6.00	110.80	3.33
Max O3	101.19	19.65	18.89	87.44	100.00	114.00	184.00	26.56

Bibliography

Brochu, Eric, Vlad M Cora, and Nando De Freitas (2010). "A tutorial on Bayesian optimization of expensive cost functions, with application to active user modeling and hierarchical reinforcement learning". In: Preprint, Viewed 16 April 2022. URL: https://arxiv.org/abs/1012.2599.

Canto, John G. et al. (2012). "Association of Age and Sex With Myocardial Infarction Symptom Presentation and In-Hospital Mortality". In: *JAMA* 307.8, pp. 813–822. DOI: 10.1001/jama.2012.199.

Catalonia, Statistical Institute of (2023a). *Air Quality Data*. Accessed: June 23, 2024. URL: https://analisi.transparenciacatalunya.cat/en/Medi-Ambient/Qualitat-de-l-aire-als-punts-de-mesurament-manuals/qg74-87s9/about_data.

— (2023b). *Census Data*. Accessed: June 23, 2024. URL: https://www.idescat.cat/pub/?id=ep&lang=en.

— (2023c). *Meteorological Data*. Accessed: June 23, 2024. URL: https://analisi.transparenciacatalunya.cat/en/Medi-Ambient/Dades-meteorol-giques-de-la-XEMA/nzvn-apee/about_data.

De Sa, Christopher (2020). *Lecture 14: Hyperparameter Optimization*. Lecture notes, CS4787 — Principles of Large-Scale Machine Learning Systems, Cornell University, Delivered 2020. URL: https://www.cs.cornell.edu/courses/cs4787/2020sp/lectures/Lecture14.pdf.

Freeborough, Warren and Terence van Zyl (Jan. 2022). "Investigating Explainability Methods in Recurrent Neural Network Architectures for Financial Time Series Data". In: *Applied Sciences* 12, p. 1427. DOI: 10.3390/app12031427.

Hrnjica, Bahrudin and Ognjen Bonacci (May 2019). "Lake Level Prediction using Feed Forward and Recurrent Neural Networks". In: *Water Resources Management*, pp. 1–14. DOI: 10.1007/s11269-019-02255-2.

Mechanic, OJ, M Gavin, and SA Grossman (2024). "Acute Myocardial Infarction". In: *StatPearls*. [Updated 2023 Sep 3]. Available from: https://www.ncbi.nlm.nih.gov/books/NBK459269/.

Mehta, Rajendra H et al. (2001). "Acute myocardial infarction in the elderly: differences by age". In: *Journal of the American College of Cardiology* 38.3, pp. 736–741. DOI: 10.1016/S0735-1097(01)01432-2. eprint: https://www.jacc.org/doi/pdf/10.1016/S0735-1097%2801%2901432-2. URL: https://www.jacc.org/doi/abs/10.1016/S0735-1097%2801%2901432-2.

Molnar, Christoph (2022). *Interpretable Machine Learning. A Guide for Making Black Box Models Explainable*. 2nd ed. URL: https://christophm.github.io/interpretable-ml-book.

Olah, Chris (2015). *Understanding LSTM Networks*. Accessed: 2024-06-19. URL: https://colah.github.io/posts/2015-08-Understanding-LSTMs/.

O'Malley, Tom et al. (2019). *KerasTuner*. https://github.com/keras-team/keras-tuner.

Peixeiro, Marco (2022). *Time Series Forecasting in Python*. Shelter Island, NY: Manning Publications. ISBN: 9781617299889.

Shumway, Robert and David Stoffer (Jan. 2011). *Time Series Analysis and Its Applications With R Examples*. Vol. 9. ISBN: 978-1-4419-7864-6. DOI: 10.1007/978-1-4419-7865-3.

Wu, Jia et al. (2019). "Hyperparameter optimization for machine learning models based on Bayesian optimization". In: *Journal of Electronic Science and Technology* 17.1, pp. 26–40.

Zhang, Zefeng et al. (2012). "Age-Specific Gender Differences in In-Hospital Mortality by Type of Acute Myocardial Infarction". In: *The American Journal of Cardiology* 109.8, pp. 1097–1103. ISSN: 0002-9149. DOI: https://doi.org/10.1016/j.amjcard.2011.12.001. URL: https://www.sciencedirect.com/science/article/pii/S0002914911035119.

Čulić, Viktor et al. (2002). "Symptom presentation of acute myocardial infarction: Influence of sex, age, and risk factors". In: *American Heart Journal* 144.6, pp. 1012–1017. ISSN: 0002-8703. DOI: https://doi.org/10.1067/mhj.2002.125625. URL: https://www.sciencedirect.com/science/article/pii/S0002870302002259.